JCIM JOURNAL OF CHEMICAL INFORMATION AND MODELING

Article

Cite This: J. Chem. Inf. Model. 2019, 59, 316−325

pubs.acs.org/jcim

Theoretical Investigation of the Structural Characteristics in the Active State of Akt1 Kinase

Lanxuan Liu, Shuobing Fan, Wenjuan Li, Wentao Tao, Ting Shi,* and Yi-Lei Zhao*

State Key Laboratory of Microbial Metabolism, Joint International Research Laboratory of Metabolic and Developmental Sciences, School of Life Sciences and Biotechnology, Shanghai Jiao Tong University, 800 Dongchuan Road, Shanghai 200240, China

Supporting Information

ABSTRACT: Akt (known as protein kinase B or PKB) is a serine/threonine kinase that regulates multiple biological processes, including cell growth, survival, and differentiation. Akt plays a critical role in the intracellular signaling network through conformational changes responsive to diverse signal inputs, and dysregulation of Akt activity could give rise to a number of diseases. However, understanding of Akt's dynamic structures and conformational transitions between active and inactive states remains unclear. In this work, classical MD simulations and QM/MM calculations were carried out to unveil the structural characteristics of Akt1, especially in its active state. The doubly protonated H194 was investigated, and both ATP−Akt1 and ADP−Akt1 complexes were constructed to demonstrate the significance of ATP in maintaining the ATP−K179−E198 salt bridge and the corresponding allosteric pathway. Besides, conformational transitions from the inactive state to the active state showed different permeation patterns of water molecules in the ATP pocket. The coordination modes of Mg^{2+} in the dominant representative conformations (I and I') are presented. Unlike the water-free conformation I', three water molecules appear around Mg^{2+} in the water-occupied conformation I, which can finally exert an influence on the catalytic mechanism of Akt1. Furthermore, QM/MM calculations were performed to study the phosphoryl-transfer reaction of Akt1. The transfer of ATP γ-phosphate was achieved through a reversible conformational change from the reactant to a critical prereaction state, with a water molecule moving into the reaction center to coordinate with Mg^{2+}, after which the γ-phosphate group was transferred from ATP to the substrate. Taken together, our results elucidate the structural characteristics of the Akt1 active state and shed new light on the catalytic mechanism of Akt kinases.

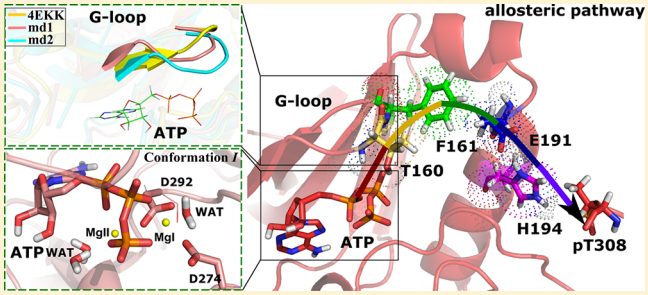

INTRODUCTION

As a serine/threonine kinase, Akt (also called protein kinase B or PKB) regulates multiple biological processes by post-translational phosphorylation of serine or threonine residues.[1] Akt is encoded by a proto-oncogene, and malfunction of its regulatory machinery often leads to various diseases and disorders, including cancers, diabetes, cardiovascular diseases, insulin resistance and type-2 diabetes, inflammatory and autoimmune disorders, and neuronal disorders.[2] Frequent activation of Akt has been reported in various human cancers, such as glioblastoma,[3] ovarian carcinoma,[4] breast carcinoma,[5] nonsmall cell lung carcinoma,[6] hematological malignancies,[7] etc. Akt activation has been shown to correlate with advanced disease and/or poor prognosis in some of these cancer types,[3,8] and inhibitors developed to suppress Akt activation have shown significant clinical potential to improve therapeutic strategies.[9] The design of ATP-competitive inhibitors in the active site of Akt kinases as anticancer agents has attracted great research interest,[10−12] and thorough explorations of the Akt active state at the atomic level for further drug development are still desired nowadays.

Activation of Akt is triggered by the production of phosphatidylinositol (3,4,5)-triphosphate (PIP_3) through upstream phosphoinositide 3-kinase (PI3K) activation.[13] Three types of Akt kinases have been identified, namely, Akt1, Akt2, and Akt3, which share above 80% sequence identity.[14] All three Akt kinases consist of an N-terminal PH-linking domain, a central kinase domain, and a C-terminal regulatory domain.[15] The Akt kinase domain is divided into two parts, the N-terminal small lobe and the C-terminal large lobe, which together constitute a nucleotide-binding pocket (Figure 1A). The N-lobe consists of five antiparallel β-sheets (the β1−5 strands) and two α-helices (the αB and αC helices). A glycine-rich loop (G-loop), located between the β1 and β2 strands, shadows the phosphate groups of ATP and contributes to phosphoryl transfer. The C-lobe is mainly composed of α-helices, and the dynamics of significant structural elements of both the N-lobe and C-lobe have been addressed.[16] The conserved Asp-Phe-Gly (DFG) sequence, which directly binds to active-site Mg^{2+} ions, is extremely important for catalysis.[17]

Received: July 26, 2018
Published: December 20, 2018

DOI: 10.1021/acs.jcim.8b00506
J. Chem. Inf. Model. 2019, 59, 316−325

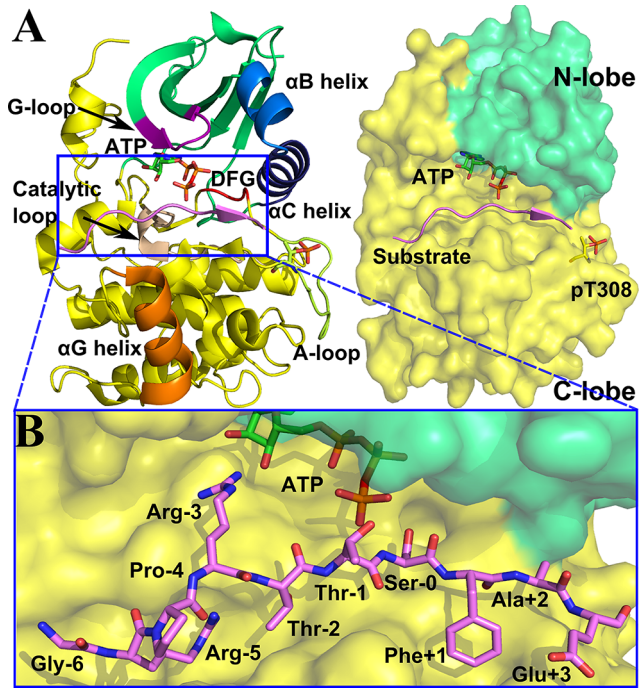

Figure 1. (A) Crystal structure of Akt1 (PDB entry 4EKK,[26] where AMP-PNP was replaced by ATP). The N-lobe and C-lobe are shown as green and yellow surfaces, respectively. ATP and pT308 are shown as sticks. Key structural elements are indicated by different colors in cartoon. (B) The substrate peptide is shown as sticks.

Conformational changes of Akt include αC-in/αC-out, DFG-in/DFG-out, and structural transformations in the G-loop, activation loop, pT308, and hydrophobic motif. There are two phosphorylation sites in Akt1: T308 in the A-loop and S473 in the hydrophobic motif.[18] Although only 10% of the reactive ability is retained in monophosphorylated pT308 Akt compared with the fully activated diphosphorylated state, phosphorylation of T308 is essential in Akt catalysis.[19] Besides, pT308 can also resist dephosphorylation by interacting with H194 in the αC helix and R273 (YRD motif) in the catalytic loop.[20] Over 100 Akt substrates have been reported since the first substrate, glycogen synthase kinase 3 (GSK3).[21] Akt1 tends to recognize substrate peptide sequences of the form RXRXX(S/T)(Hyd) and conduct phosphorylation on site (S/T) at the P(0) position, arginine (R) at P(−3) and P(−5), and a hydrophobic residue (phenylalanine) at P(+1) (Figure 1B).[19]

To date, numerous crystal structures have provided static information for studying the protein dynamics of general kinases in both active and inactive states.[22−25] ATP-dependent allosteric regulation of Akt phosphorylation has already been studied extensively using both computational and experimental methods.[20,26−28] Cheng and Niv[16] studied both phosphorylated and dephosphorylated forms of Akt to reveal the differentiated motion patterns and the crucial role of the protonation state of H196 in the active conformation. Chan et al.[20] reported that targeting Akt kinase to the cell membrane could protect it from phosphatase, which was further amplified by occupancy of the ATP binding pocket with ATP or ATP-competitive inhibitors. Lu et al.[27] and Mou et al.[28] also demonstrated similar protection effects, where ATP or ATP-competitive inhibitors could be utilized to stabilize the active-state conformation, and the corresponding allosteric pathway in Akt1 (ATP/GDC-0068 → T160 → F161 → E191 → H194 → pT308) was proposed.

In the present work, classical molecular dynamics (MD) simulations and quantum mechanics/molecular mechanics (QM/MM) calculations were carried out to explore the conformational characteristics of the active state of Akt1 kinase. Functions of the polar hydrogen atoms in the imidazole of H194 with different protonation states of Akt1 were studied. The ADP−Akt1 system was compared with ATP−Akt1 to investigate the influence of the γ-phosphate group on the ATP−K179−E198 salt bridge and the allosteric pathway. Conformational transitions from inactive states to active states were captured, and three conformations were employed to present the dynamical variations. The structural characteristics of representative conformations (I and I') were analyzed, and the mechanism of the Akt1 phosphoryl-transfer reaction was explored by QM/MM calculations.

MATERIALS AND METHODS

System Preparation and MD Simulations. The initial protein structure of ATP-bound Akt1 complex was obtained from X-ray crystal data (with AMP-PNP, Mg^{2+}, and substrate peptide; PDB entry 4EKK), and AMP-PNP was replaced by ATP.[26] Three systems with different His194 protonation states (HID, HIE, and HIP) were constructed. The ADP-bonded structure was generated through removal of the γ-phosphate of ATP from the HIP complex. Parameter preparation for Akt1 was carried out using the ff12SB force field in the AMBER 12 package.[29] Force field parameters for ATP, ADP, pT308, and Mg^{2+} ion are available in the AMBER parameter database. The protonation states of residues at pH 7.0 were determined by the PDB2PQR web server,[30] and pK_a calculations were performed using PROPKA.[31−33] The protein was externally solvated in an octahedral box of TIP3P water molecules with a 10 Å buffering distance. Sodium ions were then added as counterions to maintain system neutrality.

The solvated system was subjected to 10 000 steps of steepest-descent energy minimization followed by 1000 cycles of conjugate-gradient minimization. Then gradual heating of the whole system from 0 to 300 K in 50 ps controlled by Langevin dynamics was carried out with a 2 ps temperature collision constant. Positional harmonic restraints were imposed on the protein and ligand using a force constant of 5 kcal mol^{-1} Å^{-2}. Thereafter, a 50 ps equilibration was carried out at constant pressure and temperature (*NPT* ensemble) to adjust the density of the system to the experimental level. Following equilibration, simulations were performed in the *NPT* ensemble at 300 K and 1 atm.[34,35] During simulations, the time step was set to 2 fs, and the lengths of all chemical bonds involving hydrogen atoms were constrained with the SHAKE algorithm.[36] The cutoff of nonbonded interactions was set to 10.0 Å, and the particle mesh Ewald (PME) algorithm was employed to handle long-range electrostatic interactions.[37] The aforementioned protocol was applied to all of the simulation systems used in this study.

Trajectories were analyzed with the *cpptraj* module implanted in AmberTools14.[28] Root-mean-square deviations (RMSDs) and root-mean-square fluctuations (RMSFs) of C_α, C, and N atoms in the whole system were calculated for all MD trajectory frames. The stability of a hydrogen bond was measured by the frequency of its appearance in the entire trajectory (the acceptor−donor cutoff distance was set to 3.0 Å, and the acceptor−hydrogen−donor cutoff angle was set to

DOI: 10.1021/acs.jcim.8b00506
J. Chem. Inf. Model. 2019, 59, 316−325

135°). Clustering calculations using the average-linkage algorithms were performed to assign frames from the trajectory into different categories according to their structural similarity, and representative structures of each cluster were further studied.[38]

QM/MM Calculations. The ONIOM[39] calculations were performed with the Gaussian 09 software.[40] Representative conformations of the dominant cluster in MD trajectories were extracted as reactants (denoted as R and R′) and subjected to geometry optimization and energy calculations. A structural superimposition between the crystal structure (inactive state) and the representative conformation (active state) is shown in Figure S1. The QM region consisted of the sugar ribose and triphosphate of ATP, two Mg^{2+} ions, six residues (T160, K179, D274, K276, N279, and D292), the substrate serine at P(0), and four water molecules in close interaction with the active site (Figure S2). The total system had a net charge of −3 and 10 257 atoms, with 1698 solvent water molecules. The 114-atom QM model, bearing zero net charge, was treated with the M06-2X hybrid functional[41] and the 6-31G(d) basis set. The MM region was treated with an Amber-type force field.[42] The link atom scheme was used to partition the QM and MM regions.[43] To generate the conformation of the intermediate (prereaction state), the distance between $O_{3\gamma}$ of ATP and the Mg^{2+} ion (MgII) was scanned from 2.00 to 4.00 Å with 0.1 Å as the interval step. During this process, one water molecule gradually approached the MgII, and finally the $O_{3\gamma}$ atom was liberated from the constraint of MgII. The intermediate structure was obtained through full optimization of the last scanned structure, and the final distance between $O_{3\gamma}$ of ATP and MgII was 4.03 Å. In addition, the transition state (TS1) was located at a distance of 2.70 Å. Similarly, the P_γ atom drew near to the O_{sub} atom of the substrate to form a P−O bond, accompanied by the transfer of the phosphoryl group by breaking of the O_β−P_γ bond. The scanned distances ranged from 3.90 to 2.00 Å, and in the optimized product structure, the P−O bond length was 1.66 Å. Also, TS2 was located at 2.40 Å. All of the optimizations were performed at the M06-2X/6-31G(d) level (Figure S3).

RESULTS AND DISCUSSION

Protonated States of His194. In previous studies, the essential role of H194 in Akt1 was uncovered through experimental mutagenesis, i.e., the H194A mutant revealed markedly reduced T308 phosphorylation levels.[20] Structural analyses indicated that the H194A mutation caused pT308 to be exposed from the catalytic cleft and become accessible to phosphatase. On the other hand, different pK_a values of H194 in Akt1 kinase (PDB entry 4EKK) under physiological conditions (pH 7.0) were calculated to be 9.0, 7.7, and 6.8 by H++,[44] Accelrys,[45] and PDB2PQR,[30] respectively. The first two values correspond to doubly protonated H194 under physiological conditions, and these results are in accord with that reported by Cheng and Niv.[16] However, it still remains unknown how and to what extent the protonation state of H194 can affect the active conformation of Akt1.

To understand the role of H194 in Akt1 at the atomic level, we carried out 3 × 3 × 50 ns MD simulations with all possible protonation states of H194, including (1) the monoprotonated state on the δ nitrogen of imidazole (HID), (2) the monoprotonated state on the ε nitrogen (HIE), and (3) the diprotonated state on both the δ and ε nitrogens of H194 (HIP) (Figure 2A−C). Ligands such as ATP, two magnesium ions, and substrate were also considered in these systems. Calculation of RMSD values demonstrated that all nine trajectories rapidly reached equilibrium (Figure S4). In the HID system, a hydrogen bond was observed between N_δH of H194 and E191. Since E191 is located at the junction of the αB and αC helices, we speculated that the hydrogen bond would position αB and αC in the right orientation and facilitate the stability of the active conformation of Akt1. Our proposal was validated by HIE system, where the absence of hydrogen on N_δ of H194 resulted in partial uncoiling of the αB and αC helices. Through the RMSF calculation, bigger fluctuations of the αB and αC helices were observed in the HIE system than in the HID system (Figure S5), and the frequency at which residues 184−187 adopted a helix conformation dramatically decreased (Figure 2D), suggesting the key role of the hydrogen bond between HID194 and E191 in maintaining the structural stability of the αB helix. On the other side, N_εH of H194 was found to interact with the phosphate moiety of pT308 through a hydrogen bond in both the HIE and HIP systems. This hydrogen bond may play a significant role in keeping the kinase in a closed conformation and protecting pT308 from being dephosphorylated.

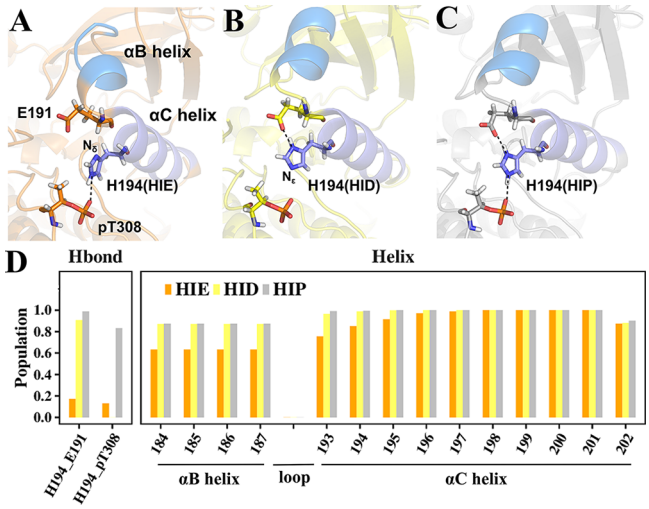

Figure 2. (A−C) Representative conformations of Akt1 in three protonation states of His194: (A) HIE, (B) HID, and (C) HIP. The αB helix is shown in marine and the αC helix in blue. (D) Proportions of hydrogen-bond formation between H194 and E191 and between H194 and pT308 as well as adoption of an α-helix conformation of residues 184−187 and 193−202 in the three systems.

On the basis of these results, it was proposed that doubly protonated H194 undertakes critical functions in the Akt1 active state: N_εH of H194 is associated with the protection of pT308, while N_δH is conducive to the maintenance of helix/structural stability by interacting with E191. Therefore, in our subsequent studies, the diprotonated His194 model was utilized to investigate the structural characteristics of the Akt1 active state.

ATP Binding and ADP Binding. Experimental results have shown that ATP can exert a protective effect on phosphorylated sites of Akt against phosphatases; ADP binding, on the other hand, may lead to a transformation of Akt from the phosphorylated (active) state into the unphosphorylated (inactive) state.[20] To investigate the role of ATP/ADP as an "on/off" switch in the catalytic cycle, the ATP−Akt1 and ADP−Akt1 complexes were constructed, and

DOI: 10.1021/acs.jcim.8b00506
J. Chem. Inf. Model. 2019, 59, 316−325

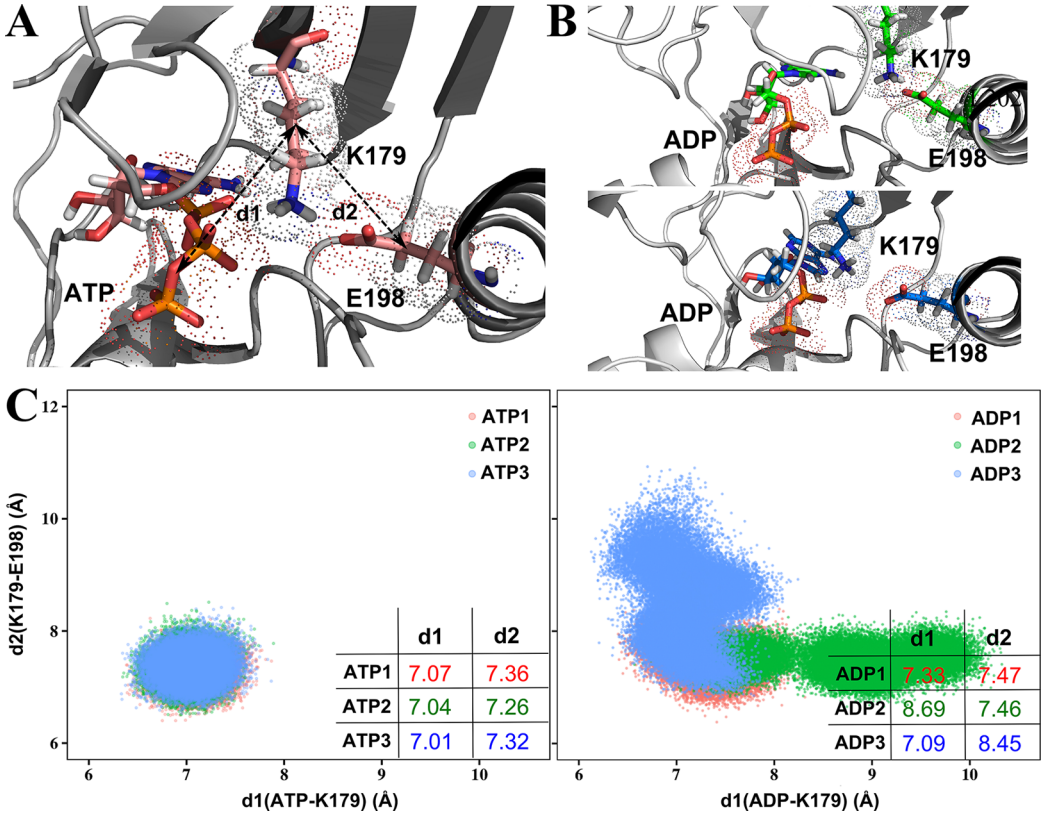

Figure 3. Representative conformations of the (A) ATP−Akt1 and (B) ADP−Akt1 systems. (C) ATP−K179 and K179−E198 salt bridge distances in three separate simulations for the (left) ATP−Akt1 and (right) ADP−Akt1 systems.

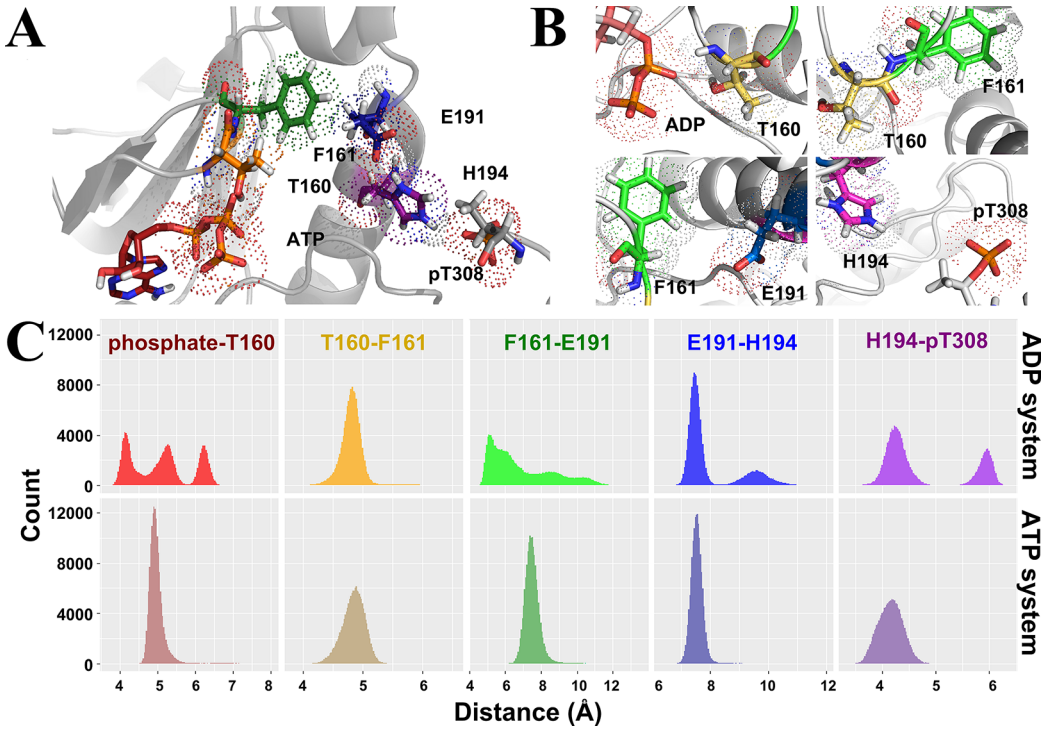

Figure 4. (A) Allosteric regulatory pathway in the ATP−Akt1 system (ATP → T160 → F161 → E191 → H194 → pT308). (B) The allosteric pathway is interrupted in the ADP−Akt1 system. (C) Distribution of distances between the residues involved in the allosteric pathway of Akt1.

3 × 100 ns MD simulations were performed on both systems. RMSD analysis suggested that all of the simulations rapidly reached their respective equilibria (Figure S6).

A conserved K179 on the rigid β3 strand was thought to interact with both the ATP α/β phosphate and E198 in the αC helix and to mediate the Akt1 reactivity by positioning ATP at

DOI: 10.1021/acs.jcim.8b00506
J. Chem. Inf. Model. 2019, 59, 316−325

a proper location, thus facilitating phosphorylation. Therefore, it is commonly believed that the ATP−K179−E198 salt bridge constitutes one of the main characteristics of the Akt1 active state.[46] In accordance with this opinion, our simulations proved that the salt bridge could be maintained well in the ATP−Akt1 system, while it became structurally unstable and ended up cracking in the ADP−Akt1 system. To be precise, the average distances between ADP and K179 were distributed in the range from 7.09 to 8.69 Å (Figure 3), while the average distance in ATP−Akt1 systems was 7.04 Å. Meanwhile, in another ADP−Akt1 trajectory, K179 stayed at a distance of 8.45 Å from E198, which is 1.14 Å longer than the average distance in the ATP−Akt1 system (7.31 Å), signifying the fracture of the salt bridge interaction. It should be noted that the distances presented here are not the direct atom-to-atom distances. Actually, the distances between the terminal heavy atoms of ATP (O_β), K179 (N_ζ), and E198 (O_δ) are close to 3 Å (Table S1). These results suggest the importance of the ATP γ-phosphate group in holding the ATP−K179−E198 salt bridge together and keeping Akt1 in an active catalytic conformation.

As illustrated by Lu et al.,[27] the allosteric regulatory pathway (ATP → T160 → F161 → E191 → H194 → pT308) plays a decisive role in protecting pT308 in the phosphorylated state. Residues involved in the pathway are scattered on different parts of Akt1P: T160 and F161 are located in the G-loop, E191 at the junction of the αB and αC helices, and H194 in the αC helix. RMSF values indicated that in comparison to the ATP−Akt1 system, these residues presented larger fluctuations in the ADP−Akt1 system (Figure S7), which might lead to a bigger conformational change and disturb the interaction in the allosteric pathway. In our study, distances between the centroids of these key residues were calculated to reveal their interactions. As shown in Figure 4, in comparison with the relative concentration of distances among these residues in the ATP−Akt1 system, the distances in the ADP−Akt1 system were distributed in a wider range, demonstrating more structural transformations. More importantly, the distances between certain residue pairs (e.g., ADP/T160, F161/E191, and H194/pT308) increased significantly, suggesting interrupted communications in the allosteric pathway. Taken together, the larger distances, the weaker interactions, and finally the less protection effect, which was validated by experimental observations,[20] demonstrate the critical role of the ATP γ-phosphate group in protecting the allosteric pathway of Akt1 phosphorylation and its catalytic bioactivity.

Flexibility of the G-Loop. It is well known that Akt1 is a very dynamic and malleable kinase with a large structural disparity between its active and inactive states. Previous studies have reported that communication between ATP and pT308 is orchestrated by the interaction between the G-loop and the αC helix.[27,28] The G-loop region (GKGTFG, residues 157−162), which is located between the β1 and β2 strands in the N-lobe, serves as a lid for the phosphates of ATP and was suggested to play an important role in both phosphoryl transfer and ATP/ADP exchange during the catalytic cycle.

Here seven separate 50 ns MD simulations were conducted in which the Akt1 crystal structure (PDB entry 4EKK), in which no interaction was present between H194 and pT308, was used as the initial structure. It was found that all seven systems rapidly reached equilibrium after 10 ns of simulation (Figure S8). Fortunately, hydrogen-bond formation between diprotonated H194 and pT308 was observed in two "active" trajectories (denoted as md1 and md2; Figure 5A); according to our previous knowledge, this hydrogen bond is indispensable for maintenance of the active state. Next, representative structures from the seven trajectories' dominant clusters were extracted and compared with the crystal structure, and the major difference was found in the G-loop (Figure 5B). In comparison with the crystal structure, the largest shift was found to be 4.32 Å, as designated by the Cα of T160, which is located at the center of the G-loop.

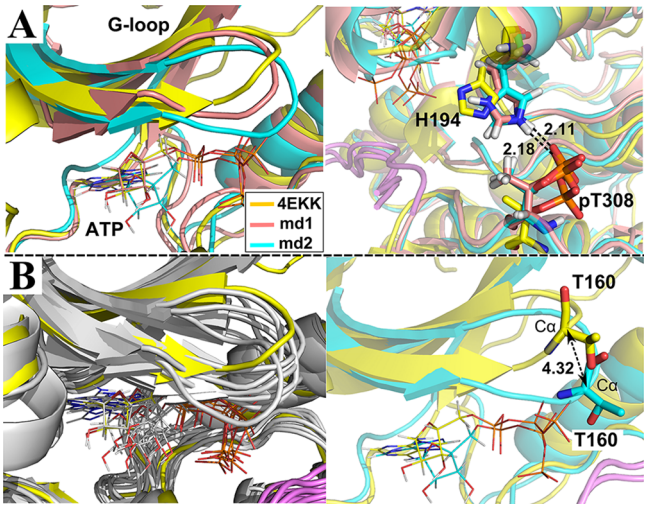

Figure 5. (A) Crystal structure of Akt1 (yellow) and representative conformations of trajectories md1 and md2 (salmon and cyan, respectively). Hydrogen bonds between H194 and pT308 are shown in black. (B) Position of the G-loop before and after simulations (yellow and gray) and the trajectory with the largest shift from the crystal structure (cyan).

Conformational Transition with Permeation of Water. Next, we prolonged the two "active" trajectories (md1 and md2) to 100 ns (Figure S9) to investigate the structural characteristics of the active state of Akt1, and three conformations (*a*, *b*, and *c*) in terms of the T160 binding mode were summarized. They could be applied to present the dynamical variations of the G-loop from the inactive state to the active state of Akt1. Especially, conformation *a* was applied to mimic the active state of Akt1, whereas conformations *b* and *c* were more likely to emphasize the "transition" process. In conformation *a* (Figure 6), the β-phosphate of ATP (O_β) clutches the hydroxyl of T160 (O_{T160}) by a hydrogen bond, exposing the γ-phosphate and further facilitating its transfer onto the substrate. In conformation *b*, O_{T160} in the G-loop is anchored to the γ-phosphate of ATP (O_γ), and as a result, ATP is fixed and shielded by the G-loop. In conformation *c*, however, the hydroxyl of T160 (O_{T160}) distances itself away from ATP and instead forms a hydrogen bond with the hydroxyl oxygen atom of serine in the substrate peptide (O_{sub}). In order to illustrate the three distinctive conformations more clearly, we used the distances d_1(O_{T160}−O_β), d_2(O_{T160}−O_γ), and d_3(O_{T160}−O_{sub}), to describe conformations *a*, *b*, and *c*, respectively. Either conformation *a* (active state) or *c* (inactive state) is quite similar between trajectories md1 and md2 (Figure S10).

As shown in Figure 6, the conformation of the Akt1 active site was transformed from *c* to *b* at 10.5 ns in trajectory md1, as indicated by the increase in d_1 from 2.80 to 4.21 Å and the

DOI: 10.1021/acs.jcim.8b00506
J. Chem. Inf. Model. 2019, 59, 316−325

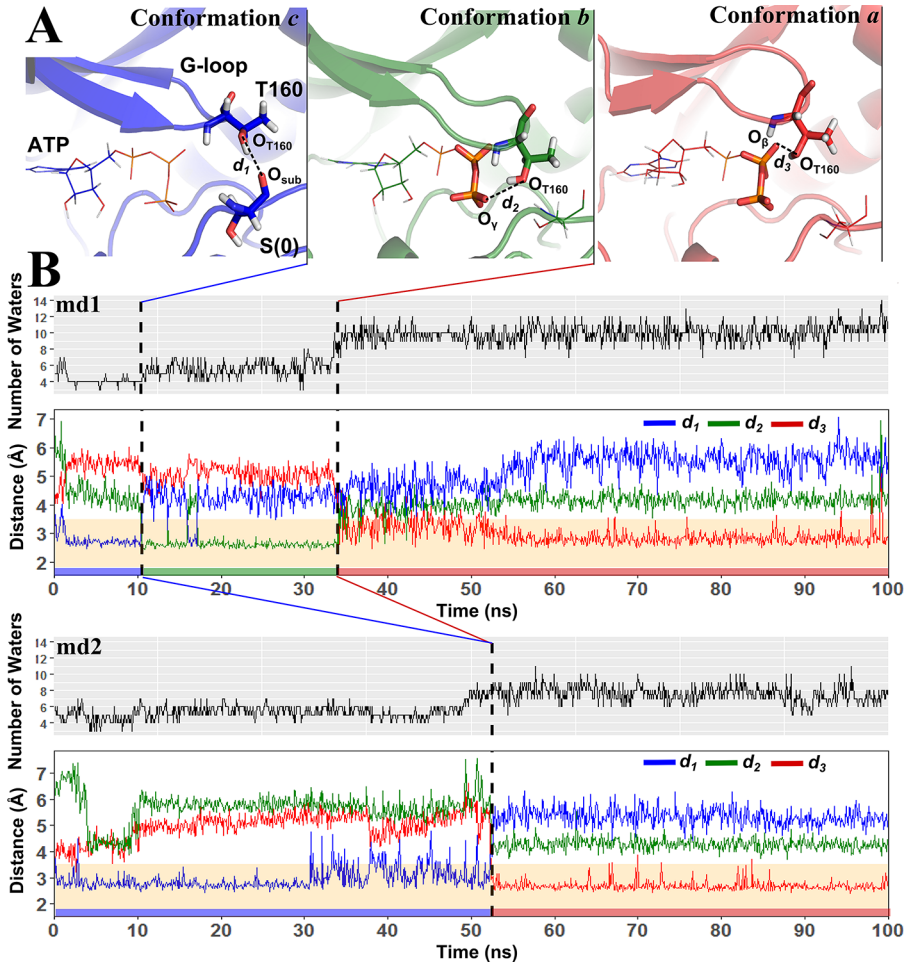

Figure 6. Analysis of the conformational transition from the inactive state to the active state of Akt1 kinase. (A) Representative conformations (*a*, *b*, and *c*) of different stages. (B) Fluctuations of the distances $d_1(O_{T160}-O_\beta)$, $d_2(O_{T160}-O_\gamma)$, and $d_3(O_{T160}-O_{sub})$ along simulations md1 and md2. The number of water molecules within 4 Å around the ATP oxygen atom bridging P_β and P_γ is also displayed. Stages of conformational change from inactive (*c*, *b*) to active (*a*) are marked with blue, green, and red colors along the trajectories, respectively.

decrease in d_2 from 4.45 to 2.68 Å. The second conformational transition from *b* to *a* occurred at 33.5 ns, when d_3 declined from 5.04 to 2.97 Å and d_2 rose from 2.68 to 4.12 Å. On the other hand, during the first 52.0 ns of simulation md2, the average of d_1 was 2.93 Å, indicating the domination of conformation *c*. Then d_1 started fluctuating violently and increased to 5.32 Å, while d_3 decreased from 4.95 to 2.71 Å, which implied that conformation *c* collapsed and was substituted by conformation *a*. Moreover, we calculated the number of water molecules in a sphere with a radius of 4 Å centered on the oxygen atom of ATP bridging P_β and P_γ. It is worthy of note that along with the conformational transition there was a massive change in the number of water molecules in the ATP pocket. In trajectory md1, for example, when conformation *b* turned into conformation *a*, the average number of water molecules increased from 5.55 to 9.92, giving us a hint that water diffusion may play a crucial role in both phosphoryl transfer and ATP/ADP exchange during the catalytic cycle.

To sum up, three typical conformations were obtained from two "active" trajectories, in which the hydrogen bond between H194 and pT308 was readily formed to ensure the sustenance of the Akt1 active state. Compared with conformation *a*, conformations *b* and *c* differed in the shape of the G-loop and the binding mode with ATP, but both of them could spontaneously transform to conformation *a*, where the hydroxyl of T160 forms a hydrogen bond with the *β*-phosphate of ATP. Moreover, following the conformational transition, water molecules flooded into the ATP pocket, which might influence the binding mode of ATP with Mg^{2+} of Akt1.

Binding Mode of Mg^{2+} Ion. Next, we carefully examined the equilibrium structures (i.e., the representative structures of the dominant clusters) obtained from trajectories md1 and md2 (conformations *I* and *I′*, respectively) (Figure 7). Although the hydrogen bond between O_{T160} of T160 and O_β of ATP was maintained in both conformations, the structures of their ATP pockets differed from each other. Besides the number of water molecules as mentioned above, the primary

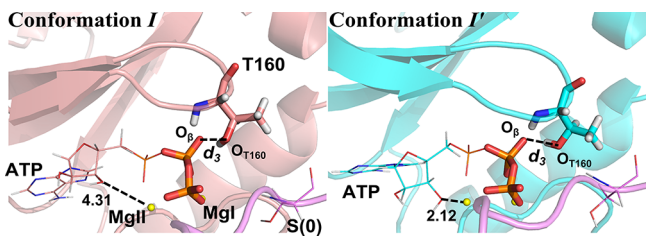

Figure 7. Conformations of the active sites obtained from simulations md1 (conformation *I*, salmon) and md2 (conformation *I′*, cyan).

DOI: 10.1021/acs.jcim.8b00506
J. Chem. Inf. Model. 2019, 59, 316−325

dissimilarity between conformations I' and I lies in the relative location between ATP and Mg^{2+}. The ribose of ATP is forced closer to the Mg^{2+} ion (MgII) in conformation I' (2.12 Å) than in conformation I (4.31 Å), resulting in different ATP−Mg^{2+} binding modes.

To be more detailed, in conformation I (Figure 8), the Mg^{2+} ion MgI is hexahedrally coordinated with $O_{\delta 2}$ of Asp274 in the

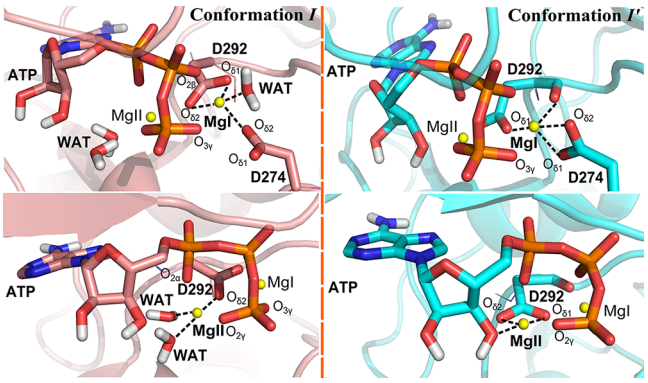

Figure 8. Coordination modes of the two Mg^{2+} ions with ATP and key residues in conformations I (salmon) and I' (cyan).

catalytic loop, $O_{\delta 1}$ and $O_{\delta 2}$ of Asp292 of the DFG motif, $O_{2\beta}$ and $O_{3\gamma}$ of ATP, and an oxygen atom from a water molecule, whereas MgII is coordinated with $O_{\delta 1}$ of Asn279, $O_{\delta 2}$ of Asp292, $O_{2\alpha}$ and $O_{2\gamma}$ of ATP, and two oxygen atoms from two water molecules. On the other hand, both carboxyl groups of Asp292 and the γ-phosphate group of ATP are drawn closer to MgII in conformation I', and as a result, Asp292 serves as a bidentate ligand to MgII and the hydroxyl oxygen on the ATP ribose occupies the remaining coordination space of MgII. In sharp contrast, three water molecules are present around Mg^{2+} in conformation I, while no water is involved in Mg^{2+} coordination in conformation I'. These structural differences would finally exert an influence on the catalytic mechanism of the Akt1 phosphoryl-transfer reaction.

Catalytic Mechanism. Our previous work indicated that the auto-phosphoryl-transfer reaction of CheA histidine kinase starts with a rapid and reversible conformational change from the ground state to a prechemistry state (i.e., a prereaction state)[47] in which the O_γ atom of ATP coordinated with the catalytic Mg^{2+} ion is replaced by an O atom from a water molecule, subsequently liberating the γ-phosphate group from the constraint of Mg^{2+} and facilitating phosphorylation of its substrate. Herein, the γ-phosphate group of ATP in either water-occupied conformation I or water-free conformation I' is coordinated with the MgII ion as well, which is unfavorable for the phosphorylation reaction. Thus, it was postulated that a similar conformational change is required in our systems. For this purpose, key structures, including the transition states (TS1 and TS2), ground states (R and R′), prereaction structures (IM and IM′), and phosphate-group-accepting polypeptide products (P and P′) corresponding to conformations I and I' were optimized at the ONIOM (M06-2X/6-31G(d):Amber) level. Our calculations focused on potential energies, and free energies are also suggested for further explorations.[48,49]

After the optimizations of the ground states, we found the water-occupied conformation I to be more stable than the water-free conformation I', and therefore, we carefully studied the phosphoryl-transfer reaction with the former system. As shown in Figure 9, the distance r(MgII−O_{wat}) was found to be 3.90 Å in the optimized reactant R and reduced to 2.04 Å in the optimized intermediate IM, while the distance r(MgII−O_γ) was initially 1.91 Å in R and enlarged to 4.03 Å in IM. These results indicated the formation of a new bond between MgII and a water molecule and breakage of the coordination interaction between MgII and the oxygen of the ATP γ-phosphate group. The transition state was obtained during the escape of O_γ from the constraint of MgII, and the energy barrier was calculated to be 9.1 kcal/mol. Since R was less

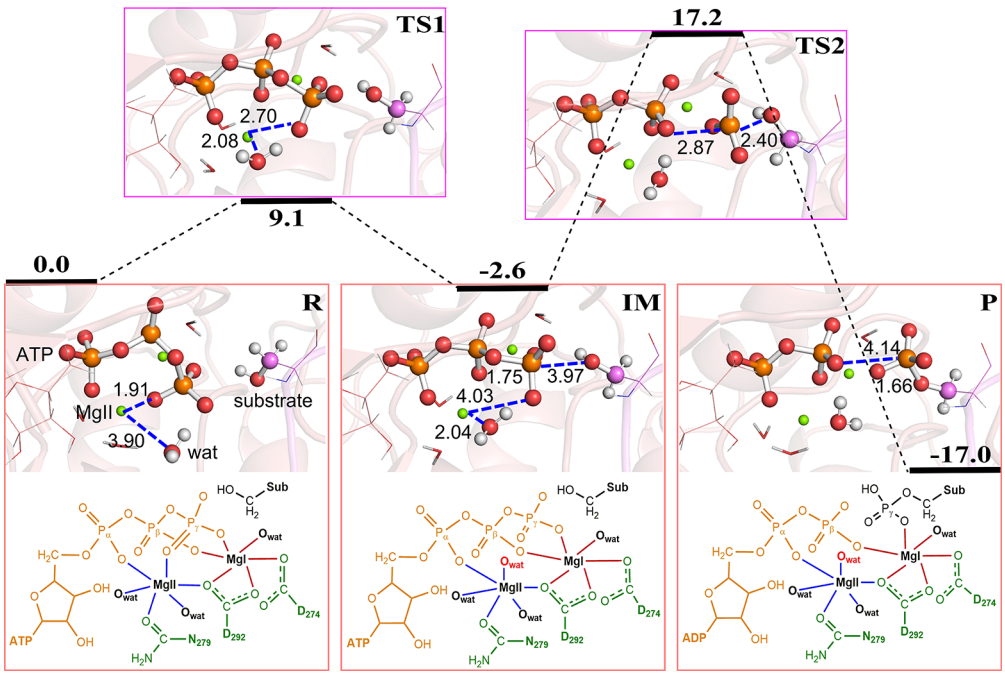

Figure 9. Potential energy profile of the proposed phosphoryl-transfer mechanism with optimized key structures of Akt1 kinase.

DOI: 10.1021/acs.jcim.8b00506
J. Chem. Inf. Model. 2019, 59, 316−325

stable than IM by only 2.6 kcal/mol, we propose that the conformational transition between R and IM might be reversible. Then the phosphoryl-transfer reaction proceeded when the γ-phosphate group of ATP conducted a nucleophilic attack, accompanied by deprotonation of the hydroxyl group of the substrate. It was found that the distance $r(P_\gamma-O_{sub})$, which represents the nucleophilic attack process, was 3.98 Å in IM and decreased to 1.66 Å in the optimized product P, indicating the formation of the $P_\gamma-O_{sub}$ bond and the completion of the phosphoryl-transfer reaction. Also, the transition state of this step was located by scanning the formation of the $P_\gamma-O_{sub}$ bond. The transfer of the ATP γ-phosphate group to the substrate was considered to be the rate-determining step with an energy barrier of 19.8 kcal/mol. It should be noted that P is more stable in energy than R by 17.0 kcal/mol (corrected to approximately 10.0 kcal/mol with a larger basis set; Table S2), suggesting the favorability of phosphor-accepting polypeptide products in thermodynamics.

Next, we conducted optimization of conformation I' (Figure S11). In IM′, a water molecule was also found to squeeze its way into the coordination site of MgII. Although the γ-phosphate group of ATP was liberated by MgII, it got caught by MgI instead, which posed another hindrance to its transfer onto the substrate. In terms of energy, IM′ was calculated to be 19.2 kcal/mol less stable than R′, indicating an unfavorable conformational change. We think that the energy discrepancy might be overestimated and could be reduced if different computational methods were considered. Finally, the energy of P′ was found to be approximately 17.0 kcal/mol more stable than R′ (Table S2), consistent with the energy gap between P and R.

Moreover, energetic corrections to all of the obtained structures at different levels of theory were performed (Table S2), and the results suggested that conformation I is energetically more favorable than conformation I', since both the reactant and the product had lower energies than R′ and P′, respectively. The conformational transformation between R and IM was easily achieved with a small energy gap of less than 3 kcal/mol, while the transition from R′ to IM′ was confronted with a relatively large barrier. To sum up, when water molecules diffused into the ATP pocket, a critical prereaction state was formed through a reversible conformational change. After the ATP γ-phosphate group escaped from the MgII-bound state to approach the substrate, the phosphoryl-transfer reaction completed.

CONCLUSIONS

To date, numerous experimental and computational studies have been conducted to decipher the catalytic mechanism of Akt1. However, the detailed structure−function interactions in the active and inactive states of Akt1 still remain unsolved. We utilized an integration of classical MD simulations and QM/MM calculations to investigate the structural characteristics of Akt1's active state. MD simulations on three protonated states of H194 revealed that $N_\varepsilon H$ of H194 can exert a protection effect on pT308 by locking pT308 in the catalytic cleft with a hydrogen bond, and $N_\delta H$ of H194 promotes the protein helix/structural stability of Akt1 by interacting with E191. In a word, the doubly protonated H194 is superior to the singly protonated states in sustaining Akt1 in its active conformation. Next, a comparison between the ADP−Akt1 and ATP−Akt1 systems was performed, and the ADP−Akt1 system was validated to be less stabilized, since both an ATP−K179−E198 salt bridge and a previously proposed allosteric pathway (ATP → T160 → F161 → E191 → H194 → pT308) tended to crack in the ADP−Akt1 system. Furthermore, seven 50 ns simulations initialized from the Akt1 crystal structure revealed the inherent flexibility of the G-loop, and two favorable trajectories were prolonged to 100 ns simulations. Three conformations (*a*, *b*, and *c*) regarding interactions between the G-loop and ATP were extracted from the trajectories. Analysis revealed conformation *a* to be the most stable, and their conformation change was always accompanied by ingress of water molecules. What is more, as a crucial part of Akt1 activation, the coordination modes of Mg^{2+} in the representative conformations I and I' was presented. Unlike the water-free conformation I', three water molecules were observed around Mg^{2+} in conformation I. Besides, the key structures R/R′, IM/IM′, and P/P′ in the phosphoryl-transfer reaction were optimized by QM/MM calculations. We propose the following Akt1 catalytic mechanism: a prereaction state is attained through a reversible conformation change from R, with a water molecule moving into the reaction center to coordinate with Mg^{2+}, while the γ-phosphate group seizes the chance and is transferred from ATP to the substrate. In summary, our study reveals the structural characteristics of the Akt1 active state and the catalytic mechanism of the γ-phosphate transfer reaction, which could help improve the understanding of structure−function relationships of Akt kinases.

ASSOCIATED CONTENT

Supporting Information

The Supporting Information is available free of charge on the ACS Publications website at DOI: 10.1021/acs.jcim.8b00506.

Structural comparison between the inactive crystal structure and the active conformation; RMSD and RMSF values for the MD simulations of the HIE, HID, and HIP systems as well as the ATP−Akt1 and ADP−Akt1 systems; distances between the terminal heavy atoms of ATP, K179, and E198; atoms of key residues included in the QM region in QM/MM calculations; potential energy paths from reactant to product; optimized key structures R′, IM′, and P′ in the phosphoryl-transfer reaction obtained from md2; and energetic corrections to the structures of conformations I and I' with the M06-2X functional and different basis sets (PDF)

AUTHOR INFORMATION

Corresponding Authors

*Tel/Fax: +86-21-34207347. E-mail: tshi@sjtu.edu.cn.
*Tel/Fax: +86-21-34207190. E-mail: yileizhao@sjtu.edu.cn.

ORCID

Yi-Lei Zhao: 0000-0003-4687-7847

Author Contributions

T.S. and Y.-L.Z. conceived and designed the investigation. L.L., W.L., W.T., and T.S. performed calculations and analyses. L.L., S.F., W.L., T.S., and Y.-L.Z. wrote the paper.

Notes

The authors declare no competing financial interest.

DOI: 10.1021/acs.jcim.8b00506
J. Chem. Inf. Model. 2019, 59, 316−325

■ ACKNOWLEDGMENTS

The authors thank the National Basic Research Program of China (973 Program) (2012CB721005) and the National High-Tech R&D Program of China (863 Program) (2012AA020403), the National Natural Science Foundation of China (21377085 and 31770070), SJTU-YG2016MS42, YG2016MS33, ZH2018ZDA26, and the SJTU-HPC computing facility award for financial support and computational time.

■ REFERENCES

(1) Lučić, I.; Rathinaswamy, M. K.; Truebestein, L.; Hamelin, D. J.; Burke, J. E.; Leonard, T. A. Conformational sampling of membranes by Akt controls its activation and inactivation. *Proc. Natl. Acad. Sci. U. S. A.* **2018**, *115*, E3940−E3949.

(2) Martini, M.; De Santis, M. C.; Braccini, L.; Gulluni, F.; Hirsch, E. PI3K/AKT signaling pathway and cancer: an updated review. *Ann. Med.* **2014**, *46*, 372−383.

(3) Chakravarti, A.; Zhai, G.; Suzuki, Y.; Sarkesh, S.; Black, P. M.; Muzikansky, A.; Loeffler, J. S. The prognostic significance of phosphatidylinositol 3-kinase pathway activation in human gliomas. *J. Clin. Oncol.* **2004**, *22*, 1926−1933.

(4) Altomare, D. A.; Wang, H. Q.; Skele, K. L.; De Rienzo, A.; Klein-Szanto, A. J.; Godwin, A. K.; Testa, J. R. AKT and mTOR phosphorylation is frequently detected in ovarian cancer and can be targeted to disrupt ovarian tumor cell growth. *Oncogene* **2004**, *23*, 5853−5857.

(5) Stål, O.; Pérez-Tenorio, G.; Åkerberg, L.; Olsson, B.; Nordenskjöld, B.; Skoog, L.; Rutqvist, L. E. Akt kinases in breast cancer and the results of adjuvant therapy. *Breast Cancer Res.* **2003**, *5*, R37−R44.

(6) Balsara, B. R.; Pei, J. M.; Mitsuuchi, Y.; Page, R.; Klein-Szanto, A.; Wang, H.; Unger, M.; Testa, J. R. Frequent activation of AKT in non-small cell lung carcinomas and preneoplastic bronchial lesions. *Carcinogenesis* **2004**, *25*, 2053−2059.

(7) Min, Y. H.; Eom, J. I.; Cheong, J. W.; Maeng, H. O.; Kim, J. Y.; Jeung, H. K.; Lee, S. T.; Lee, M. H.; Hahn, J. S.; Ko, Y. W. Constitutive phosphorylation of Akt/PKB protein in acute myeloid leukemia: its significance as a prognostic variable. *Leukemia* **2003**, *17*, 995−997.

(8) Cheong, J. W.; Eom, J. I.; Maeng, H. Y.; Lee, S. T.; Hahn, J. S.; Ko, Y. W.; Min, Y. H. Phosphatase and tensin homologue phosphorylation in the C-terminal regulatory domain is frequently observed in acute myeloid leukaemia and associated with poor clinical outcome. *Br. J. Haematol.* **2003**, *122*, 454−456.

(9) Nitulescu, G. M.; Margina, D.; Juzenas, P.; Peng, Q.; Olaru, O. T.; Saloustros, E.; Fenga, C.; Spandidos, D. A.; Libra, M.; Tsatsakis, A. M. Akt inhibitors in cancer treatment: The long journey from drug discovery to clinical use. *Int. J. Oncol.* **2016**, *48*, 869−885.

(10) Trejo-Soto, P. J.; Hernandez-Campos, A.; Romo-Mancillas, A.; Medina-Franco, J. L.; Castillo, R. In search of AKT kinase inhibitors as anticancer agents: structure-based design, docking, and molecular dynamics studies of 2,4,6-trisubstituted pyridines. *J. Biomol. Struct. Dyn.* **2018**, *36*, 423−442.

(11) Lu, J.; Zhang, Z.; Ni, Z.; Shen, H.; Tu, Z.; Liu, H.; Lu, R. QM/MM-PB/SA scoring of the interaction strength between Akt kinase and apigenin analogues. *Comput. Biol. Chem.* **2014**, *52*, 25−33.

(12) Lu, J.; Zhang, Z.; Ni, Z.; Shen, H.; Tu, Z.; Liu, H.; Lu, R.; Shi, H. The non-additive contribution of hydroxyl substituents to Akt kinase-apigenin affinity. *Mol. Simul.* **2015**, *41*, 653−662.

(13) Manning, B. D.; Toker, A. AKT/PKB Signaling: Navigating the Network. *Cell* **2017**, *169*, 381−405.

(14) Meier, F.; Schittek, B.; Busch, S.; Garbe, C.; Smalley, K.; Satyamoorthy, K.; Li, G.; Herlyn, M. The Ras/Raf/MEK/ERK and PI3K/AKT signaling pathways present molecular targets for the effective treatment of advanced melanoma. *Front. Biosci., Landmark Ed.* **2005**, *10*, 2986−3001.

(15) Liao, Y.; Hung, M.-C. Physiological regulation of Akt activity and stability. *Am. J. Transl. Res.* **2010**, *2*, 19−42.

(16) Cheng, S.; Niv, M. Y. Molecular Dynamics Simulations and Elastic Network Analysis of Protein Kinase B (Akt/PKB) Inactivation. *J. Chem. Inf. Model.* **2010**, *50*, 1602−1610.

(17) Nagar, B. c-Abl tyrosine kinase and inhibition by the cancer drug imatinib (Gleevec/STI-571). *J. Nutr.* **2007**, *137*, 1518S−1523S.

(18) Hanada, M.; Feng, J. H.; Hemmings, B. A. Structure, regulation and function of PKB/AKT - a major therapeutic target. *Biochim. Biophys. Acta, Proteins Proteomics* **2004**, *1697* (1−2), 3−16.

(19) Yang, J.; Cron, P.; Good, V. M.; Thompson, V.; Hemmings, B. A.; Barford, D. Crystal structure of an activated Akt/protein kinase B ternary complex with GSK3-peptide and AMP-PNP. *Nat. Struct. Biol.* **2002**, *9*, 940−944.

(20) Chan, T. O.; Zhang, J.; Rodeck, U.; Pascal, J. M.; Armen, R. S.; Spring, M.; Dumitru, C. D.; Myers, V.; Li, X.; Cheung, J. Y.; Feldman, A. M. Resistance of Akt kinases to dephosphorylation through ATP-dependent conformational plasticity. *Proc. Natl. Acad. Sci. U. S. A.* **2011**, *108*, E1120−E1127.

(21) Manning, B. D.; Cantley, L. C. AKT/PKB signaling: Navigating downstream. *Cell* **2007**, *129*, 1261−1274.

(22) Lauber, B. S.; Hardegger, L. A.; Asraful, A. K.; Lund, B. A.; Dumele, O.; Harder, M.; Kuhn, B.; Engh, R. A.; Diederich, F. Addressing the Glycine-Rich Loop of Protein Kinases by a Multi-Facetted Interaction Network: Inhibition of PKA and a PKB Mimic. *Chem. - Eur. J.* **2016**, *22*, 211−221.

(23) Yang, J.; Cron, P.; Thompson, V.; Good, V. M.; Hess, D.; Hemmings, B. A.; Barford, D. Molecular mechanism for the regulation of protein kinase B/Akt by hydrophobic motif phosphorylation. *Mol. Cell* **2002**, *9*, 1227−1240.

(24) Littler, D. R.; Walker, J. R.; She, Y.-M.; Finerty, P. J., Jr.; Newman, E. M.; Dhe-Paganon, S. Structure of human protein kinase C eta (PKCη) C2 domain and identification of phosphorylation sites. *Biochem. Biophys. Res. Commun.* **2006**, *349*, 1182−1189.

(25) Niefind, K.; Guerra, B.; Ermakowa, I.; Issinger, O. G. Crystal structure of human protein kinase CK2: insights into basic properties of the CK2 holoenzyme. *EMBO J.* **2001**, *20*, 5320−5331.

(26) Lin, K.; Lin, J.; Wu, W.-I.; Ballard, J.; Lee, B. B.; Gloor, S. L.; Vigers, G. P. A.; Morales, T. H.; Friedman, L. S.; Skelton, N.; Brandhuber, B. J. An ATP-Site On-Off Switch That Restricts Phosphatase Accessibility of Akt. *Sci. Signaling* **2012**, *5*, ra37.

(27) Lu, S.; Deng, R.; Jiang, H.; Song, H.; Li, S.; Shen, Q.; Huang, W.; Nussinov, R.; Yu, J.; Zhang, J. The Mechanism of ATP-Dependent Allosteric Protection of Akt Kinase Phosphorylation. *Structure* **2015**, *23*, 1725−1734.

(28) Mou, L.; Cui, T.; Liu, W.; Zhang, H.; Cai, Z.; Lu, S.; Gao, G. Microsecond molecular dynamics simulations provide insight into the ATP-competitive inhibitor-induced allosteric protection of Akt kinase phosphorylation. *Chem. Biol. Drug Des.* **2017**, *89*, 723−731.

(29) Case, D. A.; Darden, T. A.; Cheatham, T. E., III; Simmerling, C. L.; Wang, J.; Duke, R. E.; Luo, R.; Walker, R. C.; Zhang, W.; Merz, K. M.; Roberts, B.; Hayik, S.; Roitberg, A.; Seabra, G.; Swails, J.; Götz, A. W.; Kolossváry, I.; Wong, K. F.; Paesani, F.; Vanicek, J.; Wolf, R. M.; Liu, J.; Wu, X.; Brozell, S. R.; Steinbrecher, T.; Gohlke, H.; Cai, Q.; Ye, X.; Wang, J.; Hsieh, M.-J.; Cui, G.; Roe, D. R.; Mathews, D. H.; Seetin, M. G.; Salomon-Ferrer, R.; Sagui, C.; Babin, V.; Luchko, T.; Gusarov, S.; Kovalenko, A.; Kollman, P. A. *AMBER 12*; University of California: San Francisco, 2012.

(30) Dolinsky, T. J.; Nielsen, J. E.; McCammon, J. A.; Baker, N. A. PDB2PQR: an automated pipeline for the setup of Poisson−Boltzmann electrostatics calculations. *Nucleic Acids Res.* **2004**, *32*, W665−W667.

(31) Bas, D. C.; Rogers, D. M.; Jensen, J. H. Very fast prediction and rationalization of pK_a values for protein−ligand complexes. *Proteins: Struct., Funct., Genet.* **2008**, *73*, 765−783.

(32) Li, H.; Robertson, A. D.; Jensen, J. H. Very fast empirical prediction and rationalization of protein pK_a values. *Proteins: Struct., Funct., Genet.* **2005**, *61*, 704−721.

(33) Olsson, M. H. M.; Sondergaard, C. R.; Rostkowski, M.; Jensen, J. H. PROPKA3: Consistent Treatment of Internal and Surface

DOI: 10.1021/acs.jcim.8b00506
J. Chem. Inf. Model. 2019, 59, 316−325

Residues in Empirical pK_a Predictions. *J. Chem. Theory Comput.* **2011**, *7*, 525−537.
(34) Berendsen, H. J. C.; Postma, J. P. M.; van Gunsteren, W. F.; DiNola, A.; Haak, J. R. Molecular dynamics with coupling to an external bath. *J. Chem. Phys.* **1984**, *81*, 3684−3690.
(35) Uberuaga, B. P.; Anghel, M.; Voter, A. F. Synchronization of trajectories in canonical molecular-dynamics simulations: Observation, explanation, and exploitation. *J. Chem. Phys.* **2004**, *120*, 6363−6374.
(36) Ryckaert, J. P.; Ciccotti, G.; Berendsen, H. J. C. Numerical integration of the Cartesian equations of motion of a system with constraints: molecular dynamics of *n*-alkanes. *J. Comput. Phys.* **1977**, *23*, 327−341.
(37) Darden, T.; York, D.; Pedersen, L. Particle mesh Ewald: an *N*·log(*N*) method for Ewald sums in large systems. *J. Chem. Phys.* **1993**, *98*, 10089−10092.
(38) Roe, D. R.; Cheatham, T. E. III, PTRAJ and CPPTRAJ: Software for Processing and Analysis of Molecular Dynamics Trajectory Data. *J. Chem. Theory Comput.* **2013**, *9*, 3084−3095.
(39) Vreven, T.; Byun, K. S.; Komáromi, I.; Dapprich, S.; Montgomery, J. A.; Morokuma, K.; Frisch, M. J. Combining Quantum Mechanics Methods with Molecular Mechanics Methods in ONIOM. *J. Chem. Theory Comput.* **2006**, *2*, 815−826.
(40) Frisch, M. J.; Trucks, G. W.; Schlegel, H. B.; Scuseria, G. E.; Robb, M. A.; Cheeseman, J. R.; Scalmani, G.; Barone, V.; Mennucci, B.; Petersson, G. A.; Nakatsuji, H.; Caricato, M.; Li, X.; Hratchian, H. P.; Izmaylov, A. F.; Bloino, J.; Zheng, G.; Sonnenberg, J. L.; Hada, M.; Ehara, M.; Toyota, K.; Fukuda, R.; Hasegawa, J.; Ishida, M.; Nakajima, T.; Honda, Y.; Kitao, O.; Nakai, H.; Vreven, T.; Montgomery, J. A., Jr.; Peralta, J. E.; Ogliaro, F.; Bearpark, M.; Heyd, J. J.; Brothers, E.; Kudin, K. N.; Staroverov, V. N.; Kobayashi, R.; Normand, J.; Raghavachari, K.; Rendell, A.; Burant, J. C.; Iyengar, S. S.; Tomasi, J.; Cossi, M.; Rega, N.; Millam, J. M.; Klene, M.; Knox, J. E.; Cross, J. B.; Bakken, V.; Adamo, C.; Jaramillo, J.; Gomperts, R.; Stratmann, R. E.; Yazyev, O.; Austin, A. J.; Cammi, R.; Pomelli, C.; Ochterski, J. W.; Martin, R. L.; Morokuma, K.; Zakrzewski, V. G.; Voth, G. A.; Salvador, P.; Dannenberg, J. J.; Dapprich, S.; Daniels, A. D.; Farkas, Ö.; Foresman, J. B.; Ortiz, J. V.; Cioslowski, J.; Fox, D. J. *Gaussian 09*; Gaussian, Inc.: Wallingford, CT, 2009.
(41) Zhao, Y.; Truhlar, D. G. The M06 suite of density functionals for main group thermochemistry, thermochemical kinetics, noncovalent interactions, excited states, and transition elements: two new functionals and systematic testing of four M06-class functionals and 12 other functionals. *Theor. Chem. Acc.* **2008**, *120*, 215−241.
(42) Cornell, W. D.; Cieplak, P.; Bayly, C. I.; Gould, I. R.; Merz, K. M.; Ferguson, D. M.; Spellmeyer, D. C.; Fox, T.; Caldwell, J. W.; Kollman, P. A. A Second Generation Force Field for the Simulation of Proteins, Nucleic Acids, and Organic Molecules. *J. Am. Chem. Soc.* **1995**, *117*, 5179−5197.
(43) Field, M. J.; Bash, P. A.; Karplus, M. A combined quantum mechanical and molecular mechanical potential for molecular dynamics simulations. *J. Comput. Chem.* **1990**, *11*, 700−733.
(44) Gordon, J. C.; Myers, J. B.; Folta, T.; Shoja, V.; Heath, L. S.; Onufriev, A. H++: a server for estimating pK_as and adding missing hydrogens to macromolecules. *Nucleic Acids Res.* **2005**, *33*, W368−W371.
(45) Spassov, V. Z.; Yan, L. A fast and accurate computational approach to protein ionization. *Protein Sci.* **2008**, *17*, 1955−1970.
(46) Jura, N.; Zhang, X.; Endres, N. F.; Seeliger, M. A.; Schindler, T.; Kuriyan, J. Catalytic Control in the EGF Receptor and Its Connection to General Kinase Regulatory Mechanisms. *Mol. Cell* **2011**, *42*, 9−22.
(47) Shi, T.; Lu, Y.; Liu, X.; Chen, Y.; Jiang, H.; Zhang, J. Mechanism for the Autophosphorylation of CheA Histidine Kinase: QM/MM Calculations. *J. Phys. Chem. B* **2011**, *115*, 11895−11901.
(48) Smith, G. K.; Ke, Z.; Guo, H.; Hengge, A. C. Insights into the Phosphoryl Transfer Mechanism of Cyclin-Dependent Protein Kinases from ab Initio QM/MM Free-Energy Studies. *J. Phys. Chem. B* **2011**, *115*, 13713−13722.
(49) Valiev, M.; Yang, J.; Adams, J. A.; Taylor, S. S.; Weare, J. H. Phosphorylation reaction in cAPK protein kinase-free energy quantum mechanical/molecular mechanics simulations. *J. Phys. Chem. B* **2007**, *111*, 13455−13464.

DOI: 10.1021/acs.jcim.8b00506
J. Chem. Inf. Model. 2019, 59, 316−325